The trajectory, structure, and origin of the Chelyabinsk asteroidal impactor

Jiří Borovička[1], Pavel Spurný[1], Peter Brown[2,3], Paul Wiegert[2,3], Pavel Kalenda[4], David Clark[2,3] & Lukáš Shrbený[1]

[1]Astronomical Institute, Academy of Sciences of the Czech Republic, CZ-251 65 Ondřejov, Czech Republic. [2]Dept. of Physics and Astronomy, University of Western Ontario, London, Ontario, N6A 3K7, Canada. [3]Centre for Planetary Science and Exploration, University of Western Ontario, London, Ontario, N6A 5B7, Canada. [4]Institute of Rock Structure and Mechanics, Academy of Sciences of the Czech Republic, V Holešovičkách 41, CZ-18209 Praha 8, Czech Republic.

The Earth is continuously colliding with fragments of asteroids and comets of various sizes. The largest encounter in historical times occurred over the remote Tunguska river in Siberia in 1908 producing an airburst of energy 5–15 Mt TNT[1,2] (1 kt TNT = 4.185 × 10^{12} J). Until recently, the next most energetic airburst events occurred over Indonesia in 2009[3] and near the Marshall Islands in 1994[4], both having energies of several tens of kilotons. Here we analyzed selected video records of the Chelyabinsk superbolide of February 15, 2013 with energy 500 kt TNT[5]. We found statistically significant similarity of its orbit with the orbit of the 2 km asteroid 86039 (1999 NC43), suggestive of a genetic linkage. The bulk strength of the Chelyabinsk asteroid, ~1 MPa, was similar to that of smaller meteoroids[6], and corresponds to a heavily fractured single stone. The asteroid disrupted into small pieces between the heights 45–30 km above ground, saving the ground from more serious damage. The total mass of surviving fragments larger than 100 g was lower than expected[7]. We present details of the atmospheric passage, the first available for a body of such size.

The data for Tunguska are limited to tree damage and seismic/acoustic waves at large distances. The Indonesian and Marshall Islands' impacts were detected only by distant infrasonic stations or satellites in orbit and were therefore poorly documented. Some camera data exists for the multi-kiloton Sutter's Mill event[8], but precise analyses of the ablation process based on imaging have been made only for impacts of meter-sized bodies with energies of ~0.1 kt TNT[9,10,11] and smaller[12].

The Chelyabinsk impact occurred unexpectedly over a relatively densely populated Russian region during the sunrise of February 15, 2013. The superbolide generated a damaging airblast wave. An 8-meter wide hole in the ice of Lake Chebarkul, 70 km West of Chelyabinsk, was reported shortly after the event. Thousands of small meteorites of total mass >100 kg classified as LL5-ordinary chondrites were found in the areas South-Southwest from Chelyabinsk[13].

Here we determine the bolide trajectory and orbit and describe the ablation process of the asteroid. The main data for these analyses were 15 bolide videos publicly available on the internet (Extended Data Table 1) and calibrated with wide-field stellar imagery. Details of our procedure, based on the least squares method[14] are given in Supplementary Information. The trajectory and speed is presented in Table 1. The observed low deceleration provides an extreme lower limit for the mass of the body as $>10^6$ kg. The measured energy[5] and speed provide a best estimate of the mass of $\sim 1.2\times10^7$ kg, corresponding to a diameter of ~19 m, assuming bulk density of 3300 kg/m^3.

The pre-impact orbit (Table 2) is consistent with an origin in the main asteroid belt, most probably in the inner main belt near the ν_6 orbital resonance. We integrated the orbit and 1000 test particles within the orbital uncertainties (a probability cloud) 2000 years into the past. The asteroid spent the 6 weeks prior to impact within 45 degrees of the Sun, a region of the sky inaccessible to ground-based telescopes. At earlier times, the asteroid was always too faint when some portion of the probability cloud was in the field of view of existing asteroid surveys. We note that a 2.2 km diameter[15] near-Earth asteroid 86039 (1999 NC43) of Q spectral type[16] (corresponding to ordinary chondrites) has a very similar orbit, with very low dissimilarity criteria D = 0.050 [17] and D' = 0.018 [18] relative to Chelyabinsk asteroid. Though this does not provide an unequivocal dynamical link, such a close match is unlikely statistically: From Mainzer et al.[19] we expect 227 NEAs brighter than 86039 to exist. Selecting at random from the expected distribution of NEAs[20] it takes an average of 6×10^5 draws before selecting one with a smaller D, and over 3 million draws for D'. Since 227/600,000=1:2600 and 227/3,000,000=1:13,000, we conclude that there is an approximately 1:10,000 chance that the proximity of these orbits is due purely to chance. The two orbits have maintained two intersection points over the last 2000 years, one near perihelion and one near aphelion (Extended Data Fig. 1). The minimum velocity kick required

to eject Chelyabinsk from 86039 is 0.7 km/s (aphelion) or 2 km/s (perihelion). This ejection velocity is consistent with a collision with another asteroid (few km/s).

The fragmentation during atmospheric entry was studied using the bolide light curve[5] and deceleration with the procedure developed recently[11]. The arrival times of secondary sonic booms heard on videos were also used to locate fragmentation points (the primary blast wave was caused by cylindrical shock from the trajectory[5]). The dynamic pressure acting on the body was computed at each fragmentation point to evaluate the mechanical strength of the body.

The first significant mass loss occurred around a height of 45 km, under dynamic pressure 0.7 MPa. The series of most severe fragmentations occurred between 40 – 30 km (1–5 MPa). Acoustic analysis revealed 11 individual fragmentations between heights 39.2–29.8 km (Extended Data Fig. 2), the two strongest at 31.9 and 30.6 km (with uncertainties ± 0.3 km). Below 29 km height the asteroid was fragmented into ~ 20 large boulders of masses ~ 10^4 kg. Judging from the deceleration, the mass of the leading boulder (main body) was ~ 2×10^4 kg. The boulders started to break-up again at heights of 26 – 24 km (10 – 13 MPa). The main body reached a height of 22 km as a still quite massive single body (~ 10^4 kg) before severe disintegration began at a pressure of 18 MPa. Only a 15 kg fragment remained from the leading main mass at 17 km. Fragment F1, the largest individual piece surviving the flight, separated from one of the more decelerated boulders (not the main body) at a height of about 25 km, surviving a maximal dynamic pressure of 15 MPa at a height of 20 km. Its trajectory deviated from the original direction of flight (see Extended Data Fig. 3) by 1.3° ± 0.4°, implying that the lateral velocity gained at the breakup was 400 ± 130 m/s. This lateral velocity is almost an order of magnitude larger than aerodynamic theory[21] and laboratory experiments[22] predict. Nevertheless, it is in similar to the behaviour of the Morávka bolide[10], suggesting that forces other than purely aerodynamic effects are also present during the fragmentation of bolides. Based on its deceleration, the terminal mass of fragment F1 was 450 ± 50 kg and dark flight computation predicts a landing point in Lake Chebarkul, within 300 meters of the actual impact site (Extended Data Fig. 4). The predicted impact points and masses of other observed fragments (Extended Data Fig. 5) are given in Fig. 1 and Extended Data Fig. 6. Judging from the light curve shape, the total mass of surviving fragments > 100 g was maximally several percent of the original mass and probably much less. It is much less

that the pancake model predicts (>50%) and less that the separated fragments model predicts (> 10%)[7].

The fragmentation history shows that the bulk strength of the Chelyabinsk asteroid was ~1 MPa, a value typical for smaller meteoroids, confirming that there is little correlation of strength with near-Earth object size from centimetres to tens of meters scales[6]. Only the very strongest parts, representing < 1% of the original mass, had strength > 15 MPa, which may be comparable to the exceptionally strong Carancas meteoroid[23,24] and typical tensile strength of recovered stony meteorites[6]. Even in the Martian atmosphere, the body would probably separate into several large fragments before reaching the surface. It is therefore not surprising that most fresh craters on Mars are found in clusters[25].

A large dust trail was left in the atmosphere after the bolide passage. The southern and bottom sides of the trail were illuminated by the rising Sun. From northern sites the trail looked thin since only the illuminated bottom was visible, except for the first seconds, when the trail was self-luminous. The trail started at a height of 68 km. Between heights 60–26 km, the trail was thick with radius 1.0–1.8 km. A thinner trail continued to 21.5 km and a very thin part extended to 18 km. The total volume of the trail was in the order of 600 km^3 with an air mass of $\approx 5 \times 10^9$ kg. The lower edge of the thick trail was almost stationary immediately after the passage of the bolide but then moved forward in two waves as the material originally released at higher heights arrived. The velocities of these shocks were 2.8 and 1.7 km/s, respectively (Extended Data Fig. 6). Larger regions of hot material within the trail continued forward motion for some time after the bolide passage. The forward velocity of the brightest (and lowest) of several distinct hot spots (Extended Data Fig. 7) decreased from 0.7 km/s to zero during the time 1.5–4 seconds after the passage of the body. At the same time, a constant vertical velocity of 0.08 km/s was measured for this spot (Extended Data Fig. 6). The upward motion, clearly caused by buoyancy of the hot mixture of air, vapour and dust, still continued when the forward motion stopped. About 15 seconds after the bolide passage, splitting of the trail into two parallel tracks became apparent (Extended Data Fig. 8), an effect seen in high altitude luminous meteor trails and caused by convective instability leading to vortices[26]. After 50 seconds, the top of the cloud, which formed from the hot spot, was 3 km above the bottom of the trail (the trail as a whole moved about 0.5 km upwards). The maximum height of 6–7 km was reached after 3 minutes (Extended Data Fig. 9).

Based on the fragmentation strength of the Chelyabinsk asteroid we conclude that it was likely a fractured single stone and not a rubble-pile assemblage whose expected strength would be only ~25 Pa[27]. The unusually close orbital association with asteroid 86039 suggests a possible genetic connection. Detailed comparison of reflectance spectra from the Chelyabinsk meteorite and 86039 are highly desirable to explore this relationship. If the orbital association is real we would also predict a very short exposure age for Chelyabinsk relative to other LL-chondrites, as such orbital associations can only persist for a small fraction of the dynamical lifetime of an NEA.

Received ….. **accepted** …..

1. Vasilyev, N.V. The Tunguska Meteorite problem today. *Planet. Space Sci*. **46,** 129–150 (1998)
2. Boslough, M.B.E. & Crawford, D.A. Low altitude airbursts and the impact threat. *Int. J. Impact Engineering* **35**, 1441–1448 (2008)
3. Silber, E.A., Le Pichon, A. & Brown, P.G. Infrasonic detection of a near-Earth object impact over Indonesia on 8 October 2009. *Geophys. Res. Lett.* **38,** L12201 (2011)
4. McCord, T. B. *et al.* Detection of a meteoroid entry into the Earth's atmosphere on February 1, 1994. *J. Geophys. Res.* **100,** E2, 3245–3249 (1995)
5. Brown *et al*. The Chelyabinsk airburst: Implications for the Impact Hazard. *Nature*, this issue
6. Popova, O. et al. Very low strengths of interplanetary meteoroids and small asteroids. *Meteorit. Planet. Sci* **46**, 1525–1550 (2011)
7. Bland P.A. & Artiemeva N.A. Efficient disruption of small asteroids by Earth's atmosphere. *Nature* **424,** 288–291 (2003)
8. Jenniskens, P. *et al.* Radar-enabled recovery of the Sutter's Mill meteorite, a carbonaceous chondrites regolith breccia. *Science* **338,** 1583–1587 (2012)
9. Borovička J., Popova, O.P., Nemtchinov, I.V., Spurný, P. & Ceplecha, Z. Bolides produced by impacts of large meteoroids into the Earth's atmosphere: comparison of theory with observations. I. Benešov bolide dynamics and fragmentation. *Astron. Astrophys*. **334**, 713–728 (1998)
10. Borovička, J. & Kalenda P. The Morávka meteorite fall: 4. Meteoroid dynamics and fragmentation in the atmosphere. *Meteorit. Planet. Sci.* **38**, 1023–1043 (2003)

11. Borovička, J. et al. The Košice meteorite fall: Atmospheric trajectory, fragmentation, and orbit. *Meteoritics & Planetary Science,* doi: 10.1111/maps.12078 (2013)
12. Spurný P. *et al.* The Bunburra Rockhole meteorite fall in SW Australia: fireball trajectory, luminosity, dynamics, orbit, and impact position from photographic and photoelectric records. *Meteorit. Planet. Sci.* **47**, 163–185 (2012)
13. Nazarov, M.A. Chelyabinsk. *Meteoritical Bulletin* 102. http://www.lpi.usra.edu/meteor /metbull.php (2013)
14. Borovička, J. The comparison of two methods of determining meteor trajectories from photographs. *Bull. Astron. Instit. Czechoslovakia* **41,** 391–396 (1990)
15. Delbó, M., Harris, A.W., Binzel, R.P., Pravec, P. & Davies, J. K. Keck observations of near-Earth asteroids in the thermal infrared. *Icarus* **166,** 116–130 (2003)
16. Binzel, R.P. *et al.* Observed spectral properties of near-Earth objects: results for population distribution, source regions, and space weathering processes. *Icarus* **170**, 259–294 (2004)
17. Southworth, R.B. & Hawkins, G.S. Statistics of meteor streams. *Smithsonian Contributions to Astrophysics* **7,** 261–285 (1963)
18. Drummond, J.D. A test of comet and meteor shower associations. *Icarus* **45,** 545–553 (1981)
19. Mainzer, A. *et al.* NEOWISE observations of near-Earth objects: Preliminary results. *Astrophys J.* **743,** id. 156 (2011)
20. Bottke *et al.* Debiased orbital and absolute magnitude distribution of the near-Earth objects. *Icarus* **156,** 399–433 (2002)
21. Artiemeva, N.A. & Shuvalov, V.V. Motion of fragmented meteoroid through the planetary atmosphere. *J. Geophys. Res.* **106,** E2, 3297–3309 (2001)
22. Park, C. & Brown, J.D. Fragmentation and spreading of a meteor-like object. *Astron. J.* **144,** id. 184 (2012)
23. Brown, P. *et al.* Analysis of a crater-forming meteorite impact in Peru. *J. Geophys. Res.* **113**, E09007 (2008)
24. Borovička, J. & Spurný, P. The Carancas meteorite impact – Encounter with a monolithic meteoroid. *Astron. Astrophys.* **485**, L1–L4 (2008)
25. Daubar, I.J., McEwen, A.S., Byrne, S., Kennedy, M.R. & Ivanov B. The current martian cratering rate. *Icarus* **225**, 506–516 (2013)

26. Kelley, M. C., Williamson C. H. K. & Vlasov M. N. Double laminar and turbulent meteor trails observed in space and simulated in the laboratory. *J. Geophys. Res. Space Physics* 118, 3622–3625 (2013)
27. Sánchez, P. & Scheeres, D.J. The strength of regolith and rubble pile asteroids. eprint arXiv:1306.1622 (2013)
28. Everhart E. An efficient integrator that uses Gauss-Radau spacings. In Dynamics of Comets: Their Origin and Evolution, Carusi, A and Valsecchi, G. (eds), Kluwer, Dordrecht. p. 185 (1985)
29. Clark, D. & Wiegert P. A numerical comparison with the Ceplecha analytical meteoroid orbit determination method. *Meteorit. Planet. Sci.* **46**, 1217–1225 (2011)
30. Ceplecha, Z. Geometric, dynamic, orbital and photometric data on meteoroids from photographic fireball networks. *Bull. Astron. Instit. Czechoslovakia* **38,** 222–234 (1987)

Supplementary Information is available in the online version of the paper.

Acknowledgements We thank David Částek and Olga Popova and her team (Vyacheslav Emelyanenko, Anna Kartashova, Dmitry Glazachev, & Evgeny Biryukov) for providing the nocturnal in situ calibration images. We are obliged to all videographers for posting their videos on the internet. The work of JB, PS, and LS was supported by grant no. P209/11/1382 from GAČR and Praemium Academiae. The Czech institutional project was RVO:67985815. PB, PW and DC's work was supported in part by the Natural Sciences and Engineering Research Council of Canada and NASA's Meteoroid Environment Office.

Author Contributions J.B. measured most of the videos, computed bolide trajectory and velocity, analyzed atmospheric fragmentation and the dust trail. P.S. organized the calibrations, measured the calibration images and participated in interpretation. P.B. participated in the acoustic analysis and in interpretation. P.W. & D.C. performed the orbital integration, analyzed the parent body linkage and analyzed the asteroid visibility before impact. P.K. found many important videos and participated in acoustic analysis. L.S. prepared the calibrations and participated in video measurements. All authors commented on the manuscript.

Author Information Reprints and permissions information is available at www.nature.com/reprints. The authors declare no competing financial interests.

Correspondence and requests for materials should be addressed to J.B. (jiri.borovicka@asu.cas.cz).

Table 1 | Trajectory of the Chelyabinsk superbolide

Time s	Longitude deg	Latitude deg	Height km	Speed km/s
1.07	64.477	54.454	95.0	19.03
6.97	62.888	54.664	60.0	19.05
10.46	61.933	54.780	40.0	19.03
12.24	61.442	54.837	30.0	18.9
13.18	61.193	54.864	25.0	18.0
14.18	60.943	54.892	20.0	14.2
15.17	60.802	54.907	17.2	6
Fragment F1				
14.32	60.945	54.893	20.0	13.5
16.04	60.704	54.922	15.0	6.4
17.80	60.5883	54.9361	12.57	3.2

Time zero corresponds approximately to 3:20:20 UT. Coordinates are given in the WGS84 geoid system. Speed is relative to the Earth's surface. At the beginning, the acceleration by gravity was larger than deceleration by atmospheric drag. The beginning speed (19.03 ± 0.13 km/s) remained constant within 0.02 km/s down to a height 35 km. The bolide was recorded by videos between the heights 95.1 and 12.6 km, over a trajectory of total length of 272 km. The apparent radiant was changing due to Earth's gravity, starting at right ascension α = 328.28° ± 0.10° and declination δ= + 7.47° ± 0.05° at a height of 95 km and changing to α = 327.99°, δ= 7.88° at a height of 20 km. These values correspond to a local radiant azimuth *A* = 103.50°± 0.09° (East of North) and elevation *h* = 18.55° ± 0.08° and *A* = 100.63, *h* = 16.95°, respectively (note: *A* and *h* change also due to Earth's curvature). For comparison, the radiant of fragment F1 at 20 km was *A* = 101.87° ± 0.4°, *h* = 17.53° ± 0.3°.

Table 2 | The Pre-impact orbit of Chelyabinsk asteroid and the orbit of asteroid 86039 (1999 NC43)

	Chelyabinsk	86039
a (semimajor axis, AU)	1.72 ± 0.02	1.759621064 ± 6e-09
q (perihelion distance, AU)	0.738 ± 0.002	0.7403896 ± 1e-07
e (eccentricity)	0.571 ± 0.006	0.57923346 ± 6e-08
i (inclination, º)	4.98 ± 0.12	7.12312 ± 1e-05
Ω (longitude of asc. node, º)	326.459 ± 0.001	311.81880 ± 5e-05
ω(argument of perihelion, º)	107.67 ± 0.17	120.55894 ± 5e-05
perihelion passage	2012-12-31.39 ± 0.17	2014-01-17.45565 ± 2e-05

The Geocentric radiant and velocity of Chelyabinsk were: $\alpha_g = 332.82 \pm 0.11°$, $\delta_g = +0.28º \pm 0.14°$, $v_g = 15.14 \pm 0.16$ km/s. The orbit was obtained by numerical integration 60 days pre-impact with the RADAU integrator[28,29]. The orbit of 86039 was taken from JPL Horizons on June 7 2013. All angular coordinates are in equinox J2000.0.

Figure caption and Extended Data captions

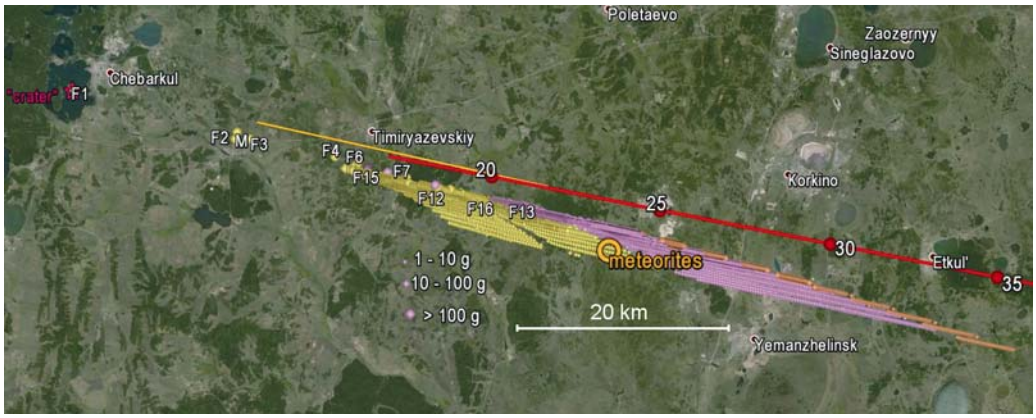

Figure 1 | **Ground projection of the terminal part of the bolide trajectory and meteorite strewn field**. The main trajectory (thick red line) and trajectory of fragment F1 (thin orange line) as plotted on Google Earth. The marks denote heights in km. The predicted impact positions of 13 observed fragments (F1–F7 and F11–F16) are shown. The impact positions of simulated small (non-observable) fragments are also given. Yellow dots denote fragments separated at lower heights (21–26 km), pink fragments originate in the main break-ups at 30–39 km and brown fragments are from above 40 km. Three dot sizes correspond to terminal masses 1–10 g, 10–100 g and above 100 g. The second largest fragment F2 had an estimated mass of 30 kg based on its observed deceleration. The dynamics after luminous flight ceased (dark flight)[30] was computed using the wind field from the nearest available radiosonde at Verkhnee Dubrovo (180 km North of Chelyabinsk) measured at 0 UT on Feb 15, 2013. Using the wind field measured by radiosonde at Kurgan (250 km East) would shift the meteorites much more to the South (by 2.5 km for a 200 g meteorite). The position of the impact hole in Lake Chebarkul ("crater") and the centroid of strewn field of small meteorites[13] are also shown. See also Extended Data Fig. 4. We expect that, as in other cases[11], the mass distribution will be more complicated and the strewn field will be larger than our idealized model predicts.

Extended Data Table 1 | List of used YouTube videos

No.	City	Longitude °E	Latitude °N	Altitude m	YouTube *code**	Author
			Videos used for trajectory determination			
1	Verkhnyaya Pyshma	60.6082	56.9635	276	LzvipPOpUy0	Vos'moy Rayon
2	Kamensk Ural'sky	61.9186	56.4151	170	kFlpCT3v12E	Aleksandr Ivanov
3	Kamensk Ural'sky	61.9333	56.3933	151	7TPDwSXaiB0	LANCER96RUS
4	Kamensk Ural'sky	61.9426	56.3852	163	J3DqsbxKOMA	LANCER96RUS
5	Chelyabinsk	61.2967	55.2204	246	4ZxXYscmgRg	Andrey Borisovich Korolev
6	Chelyabinsk	61.4720	55.1797	231	OM-5ngYg5Mg	Vyacheslav Kravchenko
7	Chelyabinsk	61.3935	55.1756	228	8Eu7QAP2DPM	Viktor Borzov
8	Chelyabinsk	61.4448	55.1663	231	32aJ4RB8MqI	MegaProfitroll
9	Chelyabinsk	61.3637	55.1500	257	gQ6Pa5Pv_io	Dmitriy Volkov
10	Korkino	61.3995	54.8909	241	odKjwrjIM-k	nek rozato
11	Yemanzhelinsk	61.3040	54.7566	234	2Gc1HgO5hNY	Aleksandr Zakharov
12	Kichigino	61.2717	54.5008	238	0CoP7WB8Gew	Mikhail Troitsk
13	Troitsk	61.5313	54.0771	183	UjNpJXP7trQ	C2Crash
14	Beloreck	58.4102	53.9527	532	5_1ytDqps8A	MrKuzaman
15	Chebarkul	60.4002	54.9950	343	xboo7LiNR08	yulya Ryzhaya
			Videos used for light curve measurement			
L1	Nizhny Tagil	59.9439	57.8703	220	NcZNhJVW5xI†	SetiTagila
L2	Tyumen'	65.6053	57.2024	60	1ZdYf2vM5LA	EastSide287
L3	Kurgan	65.2956	55.4735	70	X2ja6_zJtzk	Dmitriy Grekov
L4	Beloreck	58.4102	53.9527	532	5_1ytDqps8A	MrKuzaman
			Videos used for acoustic analysis			
A1	Chelyabinsk	55.1647	61.5482		HaMurqKMenw	Alexandr Gubarev
A2	Malinovka	55.0900	61.2500		5Rh2-v-gFEs	Svladislav74
A3	Pervomaysky	54.8726	61.2008		R99zvcrqXo8	Axel Alex
A4	Chelyabinsk	55.2675	61.4082		hMZkv0-2500	NIKI4174
A5	Chelyabinsk	55.1799	61.3479		5xMOSY4bW_M	Aleksej D
A6	Chelyabinsk	55.1570	61.3657		uXU3z3-bxNk	Andrey Yurkin
A7	Chelyabinsk	55.1500	61.3637		gQ6Pa5Pv_io	Dmitriy Volkov
A8	Chelyabinsk	55.1114	61.3509		Np_mpGYSBSA	Serg Kh
A9	Chelyabinsk	55.1650	61.4070		rflTN4XAt34	Maxim Savelyev
A10	Chelyabinsk	55.1582	61.4113		G2KpK_GmvA8	Yuriy Bazhaev
A11	Chelyabinsk	55.1570	61.4452		38zQkZCWIL0	Sergey Polyakov
A12	Chelyabinsk	55.1636	61.4703		zkVUbMdAV2Q	Alexandr Burlakov
A13	Chelyabinsk	55.1665	61.4639		QTZ0vesq5fA	greshnikacw
A14	Yemanzhelinsk	54.7564	61.3280		KmjjGgvOlMY	Daniil Lysenko
A15	Chelyabinsk	55.1404	61.4780		16KxOxjSndA	dima stepanov
A16	Kopeysk	55.1210	61.6046		VZJEfNld_JU	Aleksandr Al'shevsky
A17	Kopeysk	55.1103	61.6042		4x3xG-eKpNA	ZaTDro
A18	Kopeysk	55.1087	61.6183		UsOEy5hCCow	Andrey Kostomarov
A19	Mirnyi	54.577	60.312		LmlwWFDylx0	kaban0796

* http://www.youtube.com/watch?v=*code*
† The last of the four videos in the compilation was used

Extended Data Table 1 | List of used YouTube videos

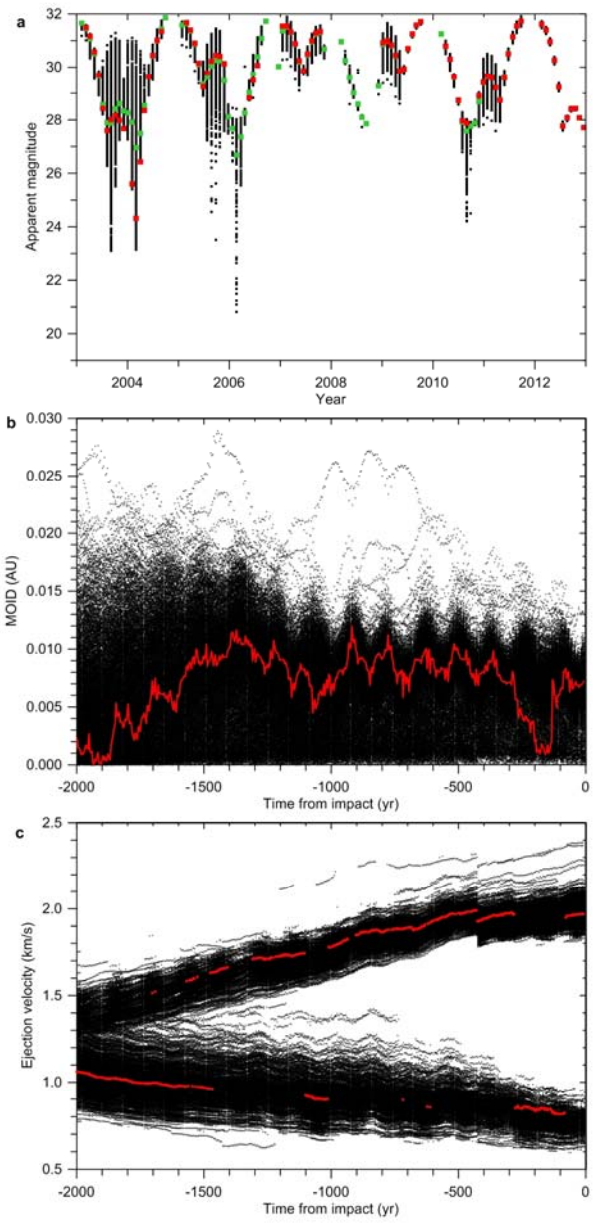

Extended Data Figure 1 | Visibility and orbital evolution of Chelyabinsk asteroid in the past. The results of backward integration of Chelyabinsk nominal orbit (red) and its 1000 clones (black dots) are presented. **a**, Apparent magnitude as seen from the Earth at 30 day intervals during last ten years. Green = mean of all clones. Plotted only for elongations > 45° from the Sun. **b,** Minimum orbit intersection distance (MOID) between the Chelyabinsk orbit and the osculating orbit of asteroid 86039 during last 2000 years. **c,** Change in velocity required to reach Chelyabinsk orbit from the orbit of 86039 at MOID during last 2000 years.

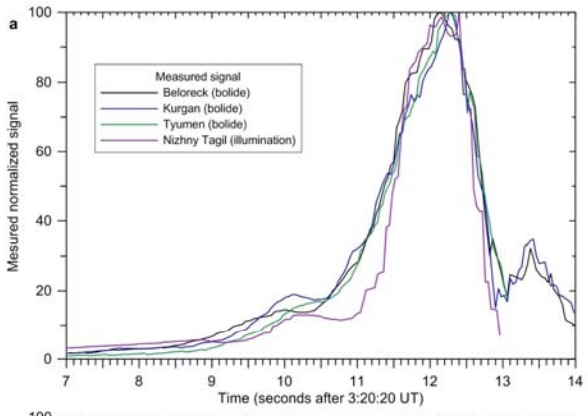

c

Heights of break-ups from sonic booms at 19 videos

42.7‡ - *39.2*† - *37.2*† - 36.4 - 35.5 - 34.9 - 33.5 - 32.6 - **31.9*** - 30.9 - **30.6*** - 29.8
25.8 - 25.5 - 21.3 - *18.6*‡ - *17.5*†

*strong
†not confirmed on video A19
‡only on video A19 but confirmed on seismic station BRVK. Another break-up suggested by BRVK at ~ 47 km.

Extended Data Figure 2 | Light curve of Chelyabinsk superbolide in relative units and heights of fragmentations as determined from sonic booms. The luminous signal was computed in relative units from pixel sum values from substantial parts of the images, and then normalized to 100. Corrections to bolide range and atmospheric extinction were applied but no attempt to convert the signal to absolute units was made (for absolute light curve see Brown et al.[5]). On each video the measured pixel sum was corrected using the estimated changes of automatic gain control of the camera. The absolute timing was obtained from the Nizhny Tagil video (L1) and the height scale from Beloreck video (14 = L4). The fragmentation heights were determined from the timing of secondary sonic booms and numerical ray tracing modelling of sonic wave's propagation from the bolide to the video sites. The used videos are listed in Extended Data Table 1. **a,** Bolide light curve as a function of time. **b,** The same data as a function of height compared with the computed source heights of sonic booms detected (as image failures) in the Mirnyi video (A19). The fragmentations are marked by vertical bars at the corresponding height. The length of the bar is proportional to the number of video frames affected by the failure. **c,** The compilation of sonic boom source heights from all 19 videos used for acoustic analysis.

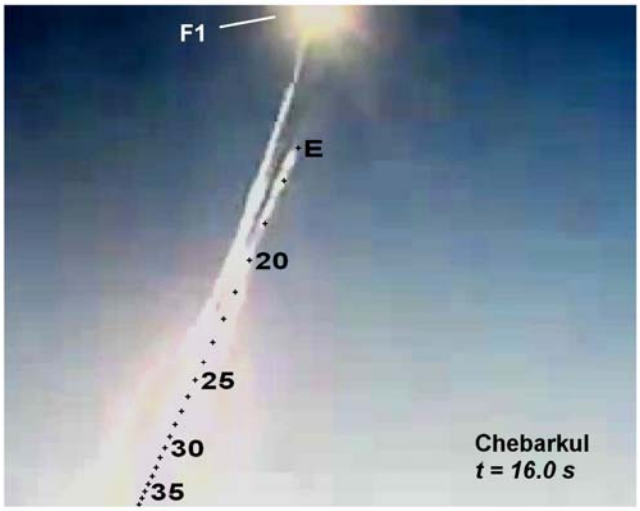

Extended Data Figure 3 | Deviation of fragment F1 from the main trajectory. Frame from video 15. The time is counted from 3:20:20 UT. The labelled marks identify points on the main trajectory at the given height (in km). E represents the endpoint of the main trajectory.

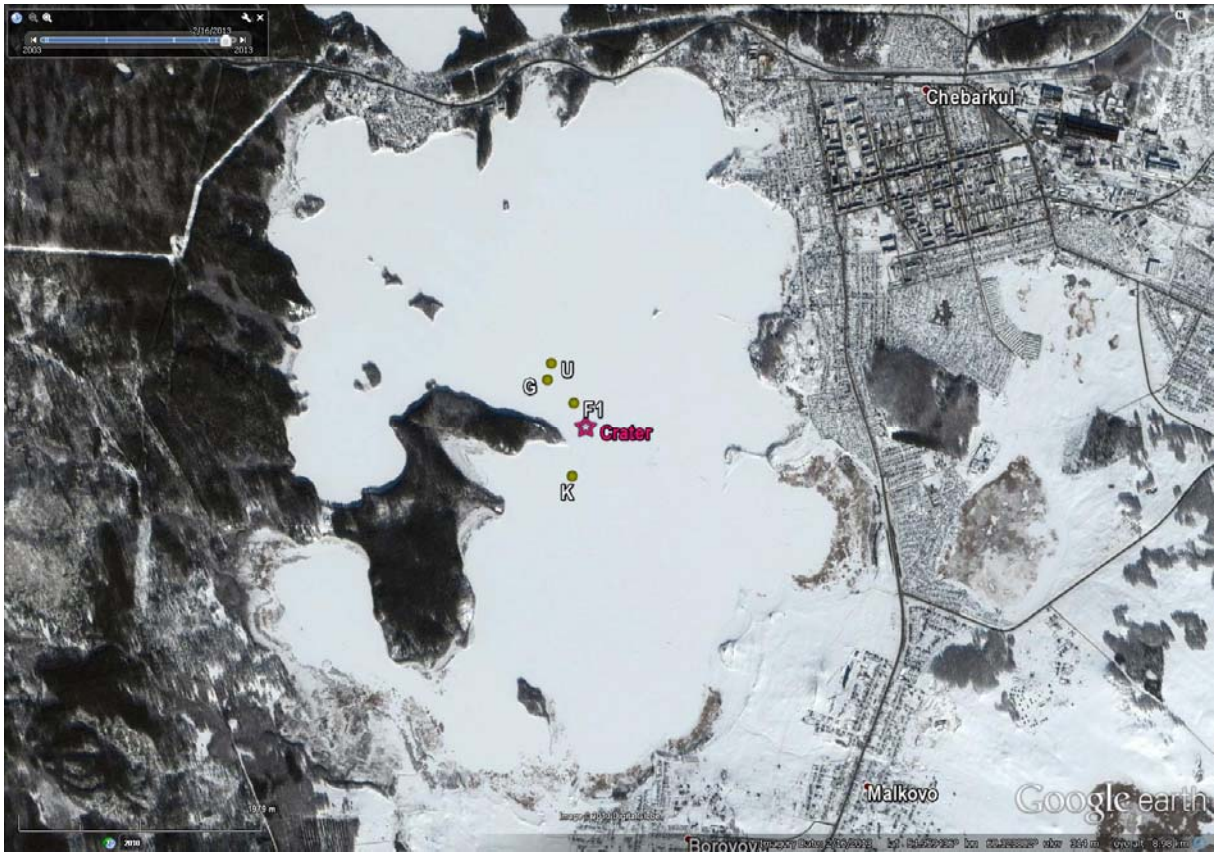

Extended Data Figure 4 | Predicted impact position of fragment F1, computed with three different wind fields, compared with the position of the hole in the ice ("crater"). The point marked F1 was computed with Verkhnee Dubrovo radiosonde data (0 UT). Point K is for Kurgan radiosonde (0 UT), point U is for UKMO wind model for Chelyabinsk (12 UT), point G with the G2S model[31] (3 UT). The distance between U and K is 960 m. The distance between F1 and crater is 260 m. Note that the position of the crater was not used for the computation of fragment F1 trajectory and impact point. The background image is from Google Earth.

Extended Data Figure 5 | Identification of fragments on a series of images from video 7. Fragments F1–F7 originated at lower heights (~ 25 km), fragments F11–F16 at upper heights (> 30 km).

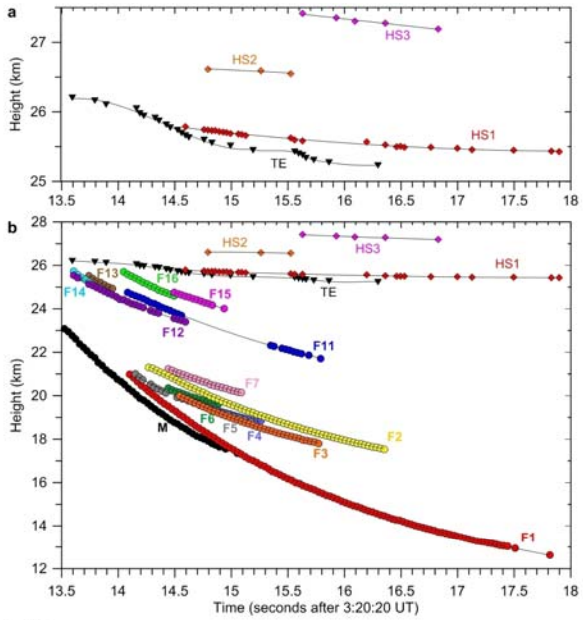

d

Fragment	Longitude °E	Latitude °N	Ablation coeff., s^2/km^2	Terminal mass, kg
M	60.5635	54.9209	0.04	15
F1	60.3194	54.9615	0.01	450
F2	60.5662	54.9268	0.05	30
F3	60.5861	54.9211	0.03	20
F4	60.7113	54.9071	0.14	3
F5	60.7572	54.8991	0.06	1
F6	60.7466	54.9019	0.05	2
F7	60.8170	54.8903	0.35	0.5
F11	60.7597	54.8980	0.09	5
F12	60.8598	54.8843	0.03	1.5
F13	60.9681	54.8666	?	0.2
F14	60.9309	54.8730	0.005	0.5
F15	60.7893	54.8945	?	5
F16	60.9583	54.8692	0.08	0.3

Extended Data Figure 6 | Dynamics of the dust trail and fragments and predicted impact positions of observed fragments. a, Height as a function of time for the lower edge of the thick dust trail (TE) and hot spots within the trail (HS1-HS3). The hot spots are identified in Extended Data Fig. 7. **b,** Height as a function of time for the main body (M), lower fragments (F1-F7), and upper fragments (F11-F16) plotted together with the dust trail features. The fragments are identified in Extended Data Fig. 5. Main body and trail were measured primarily on video 2, fragments on video 7. **c,** Upward motion of the main hot spot (HS1) within the dust trail. Vertical deviation of the centre of the hot spot from the trajectory is plotted against time. The linear fit gives upward velocity of 0.08 km/s. **d,** Predicted impact positions and dynamic properties of observed fragments. Ablation coefficients and terminal masses were obtained by fitting the observed decelerations. Masses are valid for assumed spherical shapes and bulk densities 3300 kg/m^3. In some cases the ablation coefficient could not be computed because insufficient number of data points.

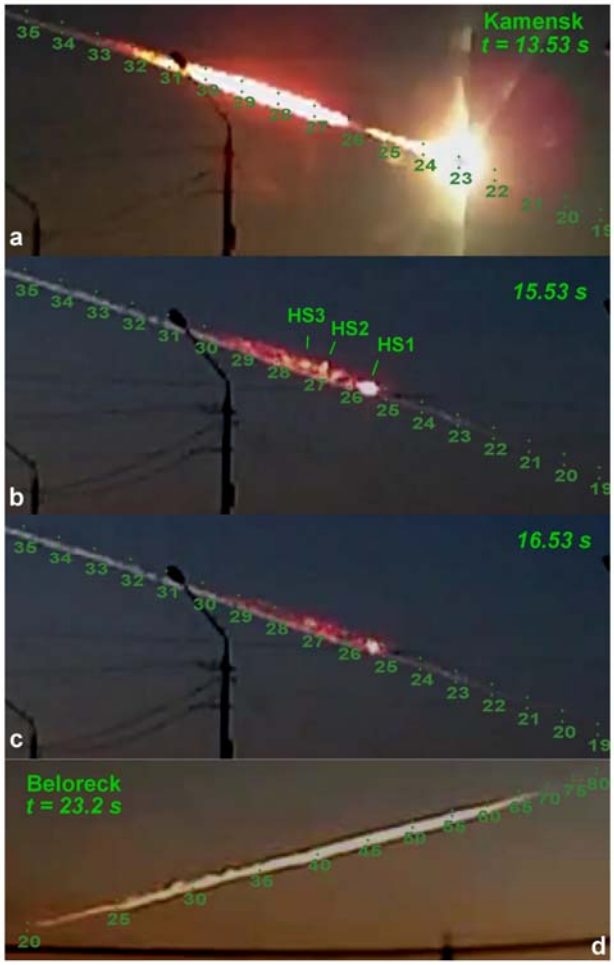

Extended Data Figure 7 | Images of the dust trail at early stages. Panels a-c are from a single video 2 located North of the fireball trajectory. Time is counted from 3:20:20 UT. Three distinct hot spots (HS1–HS3) are identified. The labelled marks identify points on the trajectory at the given height (in km). The unlabeled marks above them identify points at the same geographic coordinates but 1 km higher. They are provided to assess the width of the trail. Panel d is from video 14 from the Southwest. It demonstrates that the width of the fully illuminated fresh trail was ~ 2 km over much of its length. For later evolution of the trail see Extended Data Figs. 8 and 9.

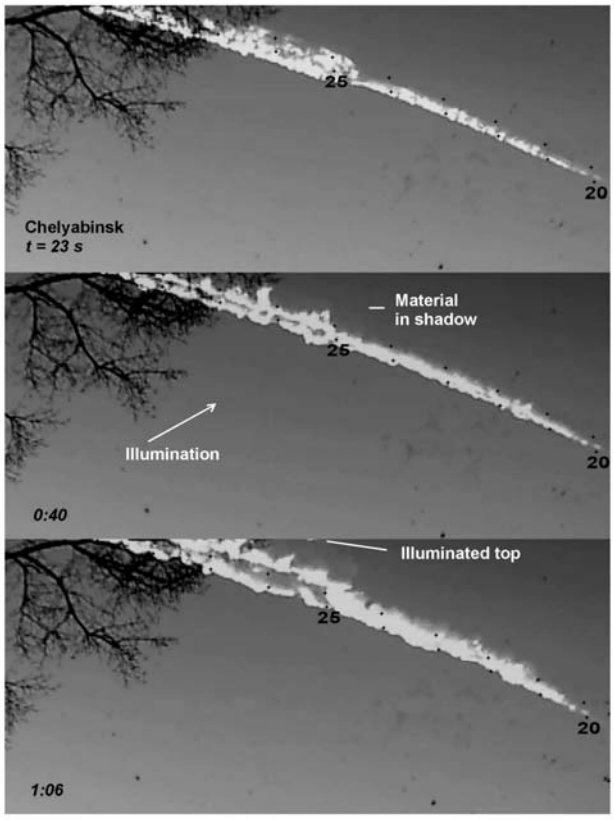

Extended Data Figure 8 | Evolution of the lower part of the dust trail as seen from Chelyabinsk during the first minute. Three frames from video 6 are given (Note: The video has colour defects). The time is given in minutes and seconds and is counted from 3:20:20 UT. The lower marks identify points on the trajectory in one km height intervals. The upper marks identify points at the same geographic coordinates but 1 km higher. The video demonstrates vertical rise and splitting of the trail. When the original video is speeded up, rotation of the material in the trail is clearly visible. The trail was illuminated from bottom. The "bubble" formed at the position of the main hot spot (HS1, see Extended Data Fig. 7) was in shadow most of the time. Only its illuminated top is visible on the third frame, just at the edge of the field of view.

Extended Data Figure 9 | Longer term evolution of the dust trail. Five frames from an uncalibrated video taken to the South of the fireball trajectory (on the road from Magnitogorsk to Chelyabinsk) are shown (source http://www.youtube.com/watch?v=Z20lnOVscpc, author Dmitriy Beleckiy). The time is given in minutes and seconds and is counted from 3:20:20 UT. The trail was fully illuminated from this site. The video demonstrates the rise of the "bubble" formed at the position of the main hot spot (HS1, see Extended Data Fig. 7). The maximal height was reached about 3 minutes after the bolide.